Science Advances

Manuscript Template

Giant oscillatory Gilbert damping in superconductor/ferromagnet/superconductor junctions

Authors

Yunyan Yao[1,2†], Ranran Cai[1,2†], Tao Yu[3], Yasumasa Tsutsumi[4], Yang Ma[1,2], Wenyu Xing[1,2], Yuan Ji[1,2], Xin-Cheng Xie[1,2,5,6], See-Hun Yang[7]*, Sadamichi Maekawa[4,8]*, and Wei Han[1,2]*

Affiliations

[1]International Center for Quantum Materials, School of Physics, Peking University, Beijing 100871, China.

[2]Collaborative Innovation Center of Quantum Matter, Beijing 100871, China.

[3]Max Planck Institute for the Structure and Dynamics of Matter, 22761 Hamburg, Germany

[4]RIKEN Center for Emergent Matter Science (CEMS), Wako 351-0198, Japan

[5]CAS Center for Excellence in Topological Quantum Computation, University of Chinese Academy of Sciences, Beijing 100190, P. R. China

[6]Beijing Academy of Quantum Information Sciences, Beijing 100193, P. R. China

[7]IBM Research - Almaden, San Jose, California 95120, USA

[8]Kavli Institute for Theoretical Sciences (KITS), University of Chinese Academy of Sciences, Beijing 100049, P. R. China

[†]These authors contributed equally to the work

*Correspondence to: weihan@pku.edu.cn (W.H.); seeyang@us.ibm.com (S.H.Y.); sadamichi.maekawa@riken.jp (S.M.).

Abstract

Interfaces between materials with differently ordered phases present unique opportunities for exotic physical properties, especially the interplay between ferromagnetism and superconductivity in the ferromagnet/superconductor heterostructures. The investigation of *zero*- and π-junctions has been of particular interest for both fundamental physical science and emerging technologies. Here, we report the experimental observation of giant oscillatory Gilbert damping in the superconducting Nb/NiFe/Nb junctions with respect to the NiFe thickness. This observation suggests an unconventional spin pumping and relaxation *via* zero-energy Andreev bound states that exist *only* in the Nb/NiFe/Nb π-junctions, but not in the Nb/NiFe/Nb *zero*-junctions, which can be qualitatively shown in a minimal model based on the Andreev bound states. Our findings could be important for further exploring the exotic physical properties of ferromagnet/superconductor heterostructures, and potential applications of ferromagnet π-junctions in quantum computing, such as half quantum flux qubits.

One sentence summary: Giant oscillatory Gilbert damping is observed in superconductor/ferromagnet/superconductor junctions with the ferromagnet thickness.

Introduction

The interplay between ferromagnetism and superconductivity have induced many exotic and exciting physical properties in ferromagnet (FM)/superconductor (SC) heterostructures (*1-3*). Of particular interest is the unconventional π-phase ground state SC/FM/SC junction that might be realized for certain FM thicknesses arising from the quantum intermixing of the wave functions between spin-singlet Cooper pairs in SC and spin-polarized electrons in FM (*1, 3, 4*). At the FM/SC interface, a Cooper pair moving into the FM will have a finite center-of-mass momentum, resulting in the oscillation of the superconducting order parameter with respect to the FM thickness (*1, 5, 6*). Depending on the FM thicknesses, the Cooper pair wavefunctions in the two superconductors on either side of the FM can have a phase difference from zero or 2π, forming so-called *zero*-junctions with positive Josephson coupling or π-junctions with the negative Josephson coupling. The FM π-junctions can be used for quantum computing applications (*7, 8*), as half quantum flux qubits (*9*). Due to the scientific and technical importance, the research on the FM π-junctions has been active for the last two decades (*6, 10-13*). Previous experimental studies have demonstrated the switching between *zero*- and π-junctions in SC/FM/SC structures by varying the temperature and the FM thickness (*11, 14-17*). These reports mainly focus on the electrical properties of the

FM *zero*- and π-junctions. However, the spin-dependent properties in FM *zero*- and π-junctions have not been explored yet. The investigation of the spin-dependent properties requires the spin current probes, such as the dynamical spin pumping (*18*). Furthemore, for the application of the FM π-junctions in quantum computing technologies (*9*), the magnetization/spin dynamic properties are extremely important to be studied.

Here, we report the experimental observation of giant oscillatory Gilbert damping in the superconducting Nb/NiFe/Nb junctions with respect to the NiFe thickness, which can be qualitatively explained by the different spin pumping efficiency via the Andreev bound states (ABS) of Nb/NiFe/Nb *zero*- and π-junctions. Using a minimal model based on the ABS, we show that an unconventional spin pumping into the zero-energy ABS could occur only for the π-junctions, which can lead to the oscillatory Gilbert damping as a function of the NiFe thicnkess.

Results

Figure 1 shows the schematic of the spin pumping, magnetization dynamics, and enhanced Gilbert damping in the SC/FM/SC heterostructures. Spin pumping refers to the spin-polarized current injection to non-magnetic materials from a FM with precessing magnetization around its ferromagnetic resonance (FMR) conditions (*19, 20*). In FM and its heterostructures, the Gilbert damping (α) characterizes the magnetization dynamics, as described by the Landau-Lifshitz-Gilbert formula with an additional Slonczewski-torque term (*21-23*):

$$\frac{d\boldsymbol{m}}{dt} = -\gamma \boldsymbol{m} \times \boldsymbol{H_{eff}} + \alpha \boldsymbol{m} \times \frac{d\boldsymbol{m}}{dt} + \frac{\gamma}{M_s V}\left(\frac{\hbar}{4\pi} g^{\uparrow\downarrow} \boldsymbol{m} \times \frac{d\boldsymbol{m}}{dt}\right) \tag{3}$$

where $\boldsymbol{m} = \boldsymbol{M}/|\boldsymbol{M}|$ is the magnetization unit vector, γ is the gyromagnetic ratio, $\boldsymbol{H_{eff}}$ is the total effective magnetic field, $M_s = |\boldsymbol{M}|$ is the saturation magnetization, and $g^{\uparrow\downarrow}$ is the interface spin mixing conductance. The pumped spin current from FM into SCs can be expressed by $\mathbf{J_s} = \frac{\hbar}{4\pi} g^{\uparrow\downarrow} \boldsymbol{M} \times \frac{d\boldsymbol{M}}{dt}$ (*20*). The reciprocal process of spin pumping is the spin transfer torque that affects the FM magnetization dynamics, which leads to an enhanced Gilbert damping constant ($\alpha_{sp} \sim J_s$)(*20*). Figure 1A depicts the pumped spin current mediated by Bogoliubov quasiparticles that reside above the superconducting gap, resulting in an enhanced Gilbert damping at elevated temperatures close to the superconducting critical temperature (T_C) (*24-28*). Figure 1B shows pumped spin current mediated by the equal-spin spin-triplet pairs ($S_z = \pm 1$) (*3*), which could enhance the Gilbert damping with heavy metals as the spin sinks adjacent to the SC, as shown in a recent experiment (*29*). Figure 1C illustrates the pumped spin current mediated by the zero-energy ABS inside the superconducting gap. The ABS can be formed within the FM layer and then extended into the interface of SCs with the superconducting coherent length scale (*30, 31*).

The SC/FM/SC junctions consist of a NiFe ($Ni_{80}Fe_{20}$) layer (thickness: ~ 5 - 20 nm) sandwiched by two Nb layers (thickness: 100 nm) grown by magnetron sputtering (see Methods and fig. S1). To maximize the integrity of samples for a systematic study, more than tens of samples are grown in each run via rotation mask technique in a sputtering system, which is the same as in the previous study of the oscillatory exchange coupling in magnetic multilayer structures (*32*). The spin transfer torque is probed via Gilbert damping measurements of Nb/NiFe/Nb junctions (see Methods for details), since the spin angular momentum transfer at the interface is proportional to the enhanced Gilbert damping (*20*).

Above the T_C of Nb, spin pumping in the Nb/NiFe/Nb junctions leads to the spin accumulation in Nb near the interface, which can be described by the spin-dependent chemical potentials, as illustrated in Fig. 2A. The Gilbert damping of NiFe in the Nb/NiFe/Nb junctions is determined from the microwave frequency-dependent FMR spectra (fig. S2). A typical FMR curve with the Lorentzian fitting is shown in Fig. 2B, from which the half linewidth (ΔH) can be obtained. The Gilbert damping can be extracted from the best linear-fitting curve of ΔH vs. f (Fig. 2C). Figure 2D shows the NiFe thickness dependence of the Gilbert damping in the Nb/NiFe/Nb junctions measured at T = 10, 15, and 20 K, respectively. Interestingly, an oscillating feature of the Gilbert damping is observed as a function of d_{NiFe} in the region of $d_{\mathrm{NiFe}} < \sim 15$ nm. This oscillating behavior can be attributed to the quantum-interference effect of angular momentum transfer between the local precessing magnetic moment and conduction electrons in thin NiFe that was theoretically predicted by Mills (*33*), but has not been experimentally reported yet. Above T_C, the continuous energy bands of Nb, similar to the normal metal in the Mills theory, overlap with both spin-up and spin-down bands of NiFe at the interface, thus allowing the conducting electrons in NiFe to flip between the spin-down and spin-up states. As illustrated in the inset of Fig. 2D, one spin-down electron scatters with the local magnetic moment and then flips to the spin-up polarization, giving rise to the angular momentum transfer between the spin-polarized electrons and the magnetic moment. Besides the change of angular momentum, the momentum of the electron also changes (Δk), due to different Fermi vectors for spin-up ($k_{F\uparrow}$) and spin-down ($k_{F\downarrow}$)

electrons with exchange splitting (Fig. 2A). When the NiFe layer is thin enough to become comparable with $\frac{1}{\Delta k}$, quantum-interference effect of the spin-polarized electrons shows up, which gives rise to the oscillating spin-transfer torque to the NiFe. When the NiFe thickness is $2n\pi/[k_{\mathrm{F}\uparrow} - k_{\mathrm{F}\downarrow}]$ (n is an integer), the matching of the quantum levels between the spin-up and spin-down electrons in NiFe induces smaller Gilbert damping. On the other hand, when the NiFe thickness is $(2\mathrm{n}+1)\pi/[k_{\mathrm{F}\uparrow} - k_{\mathrm{F}\downarrow}]$, a larger Gilbert damping is induced. Consequently, the Gilbert damping in the Nb/NiFe/Nb structures oscillates with a period of $2\pi/[k_{\mathrm{F}\uparrow} - k_{\mathrm{F}\downarrow}]$ (Supplementary Materials S1). Experimentally, an oscillating period (λ) of ~ 1.8 nm is identified (see the red dashed arrow in Fig. 2D).

Next, we investigate the spin pumping and spin transfer torque of the Nb/NiFe/Nb junctions in the superconducting states below T_C with a superconducting gap (Fig. 3A). T_C in the Nb/NiFe/Nb junctions is obtained from typical four-probe resistance measurement as a function of the temperature. A typical temperature-dependent resistance curve measured on the Nb/NiFe (12 nm)/Nb junction is shown in Fig. 3b, indicating the T_C of ~ 8.6 K. As d_{NiFe} changes, T_C of the Nb/NiFe/Nb junctions exhibits little variation between ~ 8.4 and ~ 8.9 K (fig. S3). Similar to the normal states of Nb, the Gilbert damping below T_C is also obtained from the best linear-fitting result of the half linewidth vs. frequency (fig. S4). During the FMR measurement, T_C varies a little (< 1 K) (fig. S5). As the temperature decreases, α decreases abruptly from ~ 0.012 to ~ 0.0036 across the T_C (Fig. 3C), which indicates the decrease of spin current injected into Nb due to the formation of superconducting gap below T_C. This observation is consistent with previous reports on spin pumping into SCs where the spin current is mediated by Bogoliubov quasiparticles (*24, 28, 34*). As the temperature decreases far below the T_C, the quasiparticle population dramatically decreases, leading to reduced spin pumping and Gilbert damping.

Remarkably, the oscillating amplitude of the Gilbert damping of the Nb/NiFe/Nb junctions as a function of the NiFe thickness is dramatically enhanced as the temperature decreases into the superconducting states of Nb (Fig. 3D). At T = 4 K, the oscillating magnitude of the Gilbert damping constant is ~ 0.005 for the first three oscillations, which is comparable to the background value of ~ 0.006. Such a giant oscillation of the Gilbert damping cannot be explained by spin pumping of Bogoliubov quasiparticle-mediated spin current in SCs. Since as the temperature decreases, the population of the Bogoliubov quasiparticles monotonically and rapidly decreases with an increase of the SC gap, which would lead to lower Gilbert damping and also smaller oscillation compared to the normal states. Note that the oscillating period of the Gilbert damping at $T = 4$ K is the same as that at $T = 10$ K that is supposed to be $2\pi/[k_{\mathrm{F}\uparrow} - k_{\mathrm{F}\downarrow}]$ due to the quantum interference effect. Such oscillating period of $2\pi/[k_{\mathrm{F}\uparrow} - k_{\mathrm{F}\downarrow}]$ is the also same as that of the *0*- and π-phase ground states transitions in FM Josephson devices, which is equal to the coherence length in NiFe film of $2\pi/[k_{\mathrm{F}\uparrow} - k_{\mathrm{F}\downarrow}]$ in the ballistic regime (*1, 11, 17*), and $\sqrt{\hbar D \,/\, E_{ex}}$ in the diffusive regime (D is the diffusion coefficient, and E_{ex} is the exchange energy). The observed oscillating period of ~ 1.8 nm in our study is similar to the *zero* - π oscillating period measured in the NiFe Josephson junctions in the diffusive regime reported previously (*11, 17*).

The Gilbert damping difference between the *zero*- and π-junctions is extracted as a function of NiFe thickness, as shown in Fig. 4A and fig. S6. Clearly, there is a pronounced oscillating feature of the Gilbert damping for the Nb/NiFe/Nb junctions with NiFe thickness from ~ 5 nm to ~ 11 nm. When the NiFe thickness is above ~ 11 nm, the oscillating feature of the Gilbert damping is largely suppressed compared to thinner NiFe junctions. This feature might be associated with the strong Josephson coupling for thin NiFe junctions and the exponential decaying of the Josephson coupling as the NiFe thickness increases (*11, 17*). To confirm this, the Josephson junctions are fabricated using the shadow mask technique, and a Josephson coupling is observed from the Nb/NiFe (5 nm and 10 nm)/Nb junctions (Supplementary Materials and fig. S7).

Discussion

Let us discuss the physical mechanism that induces the giant oscillating Gilbert damping in the following. As discussed above (Fig. 1), the spin current in SCs can be mediated by Bogoliubov quasiparticles, spin-triplet pairs, and ABS. Regarding Bogoliubov quasiparticles, they are populated around the superconducting gap near T_{C} due to the thermal smearing, and thus exist only at elevated temperatures close to the T_{C}. As shown both theoretical and experimental studies, the enhanced Gilbert damping in the SC/FM/SC heterostructures happens around T_{C} (*24-28*). As the temperature decreases down to 0.5 T_{C}, the Bogoliubov quasiparticles are mostly frozen out, for which the spin pumping is forbidden that will no longer contribute to the enhanced Gilbert damping. Hence, the Bogoliubov quasiparticles are very unlikely to account for our experimental results. Regarding the spin-triplet pairs, it has been shown in previous studies that the spin-triplet current under FMR conditions and spin triplet correlations would be different for *zero*- and π-

junctions (*4, 26, 35, 36*), which might result in different Gilbert damping theoretically. However, in our study, there are not spin sinks adjacent to the Nb layers, thus not allowing the spin-triplet Cooper pairs to be relaxed in the Nb. This is different from previous report on the Pt/SC/FM/SC/Pt heterostructures(*29*), where the Pt is used as the spin sink. Experimentally, as the temperature below T_C, the Gilbert damping exhibits a monotonic decrease for the Nb/NiFe/Nb heterostructures (Fig. 3C), which is different from the enhanced Gilbert damping due to spin-triplet pairs (*29*). Furthermore, no Josephson current in the Nb/NiFe/Nb heterostructures is observed in Nb/NiFe (30 nm)/Nb junction (fig.S7), indicates the absence of long range spin-triplet Josephson coupling. Both these experimental results indicate that the contribution from the spin-triplet pairs is not significant to the enhanced Gilbert damping in the superconducting Nb/NiFe/Nb junctions.

To our best understanding, the most reasonable mechanism is the spin pumping via the ABS, which can qualitatively describe our experimental observation. Previous studies have demonstrated that the energy of ABS inside the superconducting gap depends on the superconducting-phase (*37, 38*) (see Supplementary Materials S2):

$$\varepsilon_0 = \pm\Delta\sqrt{1 - D\sin^2\left(\frac{Jd_{\mathrm{NiFe}}}{\hbar v_F}\right)}, \tag{4}$$

where Δ is the magnitude of the superconducting gap, and the parameter D is the transmission coefficient which is 1 for the ideal high transparency of the junctions in the ballistic regime, J is the exchange splitting energy, and v_F is the fermi velocity. For *zero*-junctions, the distribution of the ABS is near the edge of the superconducting gap (Supplementary Materials and fig. S8A). As shown in Fig. 4B, the transfer efficiency of spin angular momentum is suppressed due to the reduced population of the ABS at low temperatures. Whileas, for the π-junctions, ABS is located around the zero-energy (Supplementary Materials and fig. S8A), thus, the spin pumping efficiency via the zero-energy ABS (Fig. 4C) can lead to an enhanced Gilbert damping. Furthermore, theoretical calculations are performed to estimate the enhanced Gilbert damping due to spin pumping via zero-energy ABS (Supplementary Materials). Fig. 4A inset shows the calculation with $D = 1$ in the ballistic regime based on the minimal theoretical model, where a large oscillating behavior of the Gilbert damping is resolved. For transmission coefficient D being less than 1, i.e., in the diffusive regime with Josephson coupling (*37, 38*), the energy level of the ABS in π-junctions locates away from zero-energy, but is still much smaller than that of the ABS in *zero*-

junctions (fig. S8A). In the very diffusive regime without Josephson coupling as NiFe thickness is much larger than its spin diffusion length, D will be almost 0. Our minimal theoretical estimation demonstrates that large oscillating Gilbert damping can be still resolved with D = 0.2 -1.0 (fig. S8B). To be noted, our theoretical estimation is based on a simplified model that assumes D does not depend on the NiFe thickness. In reality, D decreases as the NiFe thickness increases from the ballistic regime to the dirty/diffusive regime. Further theoretical studies are needed to quantitatively investigate the experimental data.

Further, the control samples of bilayer Nb/NiFe heterostructures have been investigated, for which there are no Andreev bound states or the Josephson coupling. Interestingly, these bilayer samples do not exhibit the oscillatory feature for the Gilbert damping as the NiFe thickness varies (Fig. S9). This observation further supports that the giant oscillatory Gilbert damping in the tri-layer Nb/NiFe/Nb junctions can be most likely associated with the different spin pumping efficiency into the Andreev bound states of *zero*- and π-junctions.

Materials and Methods

Materials growth

The SC/FM/SC heterostructures consisting of Nb (100 nm) and $Ni_{80}Fe_{20}$ (NiFe; ~ 5 - 20 nm) were grown on thermally oxidized Si substrates in a d.c. magnetron sputtering system with a base pressure of $\sim 1\times 10^{-8}$ torr. To systematically vary the NiFe thickness that is crucial for the quantum-size effect, we adopted the rotating multi-platter technique that allows us to grow dozens of Nb/NiFe/Nb samples in each run (*32*). The thickness of the Nb layer is fixed to be ~100 nm that is much larger than the spin diffusion length of Nb (*29, 39*). After the growth, a thin Al_2O_3 layer (~ 10 nm) was deposited *in situ* as a capping layer to avoid sample degradation against air/water exposure. The crystalline properties of Nb/NiFe/Nb heterostructures were characterized by X-ray diffraction (fig. S1A) and high-resolution cross-sectional transmission electron microscopy (fig. S1B) using a 200-kV JEOL 2010F field-emission microscope.

Ferromagnetic resonance measurement.

The spin pumping of Nb/NiFe/Nb heterostructures was characterized via ferromagnetic resonance (FMR) using the coplanar wave guide technique connected with a vector network analyzer (VNA; Agilent E5071C) in the variable temperature insert of a Physical Properties Measurement System (PPMS; Quantum Design) (*28*). The FMR spectra were characterized by measuring the amplitudes of forward complex transmission coefficients (S_{21}) as the in-plane magnetic field decreases from 4000 to 0 Oe under the microwave power of 1 mW. The typical FMR results measured on the Nb/NiFe (12 nm)/Nb heterostructures are shown in the fig. S2A (T = 10 K) and fig. S4A (T = 4 K). Weaker FMR signals are observed in the superconducting states compared to the normal states.

The half linewidth (ΔH) can be obtained by the Lorentz fitting of the magnetic field-dependent FMR signal following the relationship (figs. S2B and S4B):

$$S_{21} \propto S_0 \frac{(\Delta H)^2}{(\Delta H)^2 + (\boldsymbol{H} - \boldsymbol{H_{res}})^2} \tag{3}$$

where S_0 is the coefficient for the transmitted microwave power, $\boldsymbol{H}$ is the external in-plane magnetic field, and $\boldsymbol{H_{res}}$ is the resonance magnetic field. The Gilbert damping constant (α) can be obtained from the slope of the best linear-fitting results of the ΔH vs. the microwave frequency (*f*) (*40-43*):

$$\Delta H = \Delta H_0 + \left(\frac{2\pi\alpha}{\gamma}\right) f \tag{4}$$

where ΔH_0 is the zero-frequency line broadening that is related to the inhomogeneous properties, and γ is the gyromagnetic ratio. From the best linearly fits of the ΔH vs. f results measured on the typical Nb/Py (12 nm)/Nb sample (red lines in Figs. S2C and S4C), α is determined to be 0.012 and 0.0054 at T = 10 and 4 K, respectively. A larger zero-frequency line broadening ΔH_0 is observed for the superconducting state compared to the normal state of Nb/Py/Nb heterostructures, which could be attributed to Meissner screening effect and the formation of trapped magnetic fluxes in Nb (*43*).

Superconducting transition temperature measurement.

The superconducting transition temperature (T_C) of the Nb/NiFe/Nb heterostructures was determined via the zero-resistance temperature measured by four-probe method in a PPMS using standard a.c. lock-in technique at a low frequency of 7 Hz. The T_C of Nb (100 nm)/NiFe/Nb (100 nm) heterostructures exhibits little variation as a function of the NiFe thickness (fig. S3). It is noticed that the FMR measurement can affect the T_C a little (< 1 K), as shown in fig. S5.

Supplementary Materials

Supplementary Materials and Methods

fig. S1. The crystalline properties of the Nb/NiFe/Nb heterostructures.

fig. S2. Gilbert damping measurement of Nb/NiFe/Nb heterostructures at $T = 10$ K.

fig. S3. NiFe thickness dependence of T_C for the Nb/NiFe/Nb heterostructures.

fig. S4. Measurement of the Gilbert damping of Nb/NiFe/Nb heterostructures at $T = 4$ K.

fig. S5. The effect of FMR measurement on the T_C of Nb/NiFe/Nb heterostructures.

fig. S6. The Gilbert damping of *zero*- and π-junctions at $T = 4$ K.

fig. S7. The measurement of Josephson coupling in Nb/NiFe/Nb junctions.

fig. S8. Calculation of the enhanced Gilbert damping due to spin pumping via the ABS at $T = 4$ K.

fig. S9. Gilbert damping of control sample of bilayer Nb/NiFe junctions.

References and Notes:

1. A. I. Buzdin, Proximity effects in superconductor-ferromagnet heterostructures. *Rev. Mod. Phys.* **77**, 935-976 (2005).
2. F. S. Bergeret, A. F. Volkov, K. B. Efetov, Odd triplet superconductivity and related phenomena in superconductor-ferromagnet structures. *Rev. Mod. Phys.* **77**, 1321-1373 (2005).
3. J. Linder, J. W. A. Robinson, Superconducting spintronics. *Nat. Phys.* **11**, 307-315 (2015).
4. M. Eschrig, J. Kopu, J. C. Cuevas, G. Schön, Theory of Half-Metal/Superconductor Heterostructures. *Phys. Rev. Lett.* **90**, 137003 (2003).
5. A. I. Buzdin, L. N. Bulaevskii, S. V. Panyukov, Critical-current oscillations as a function of the exchange field and thickness of the ferromagnetic metal (F) in an SFS Josephson junction. *JETP Lett.* **35**, 178-180 (1982).
6. T. Kontos, M. Aprili, J. Lesueur, X. Grison, Inhomogeneous Superconductivity Induced in a Ferromagnet by Proximity Effect. *Phys. Rev. Lett.* **86**, 304-307 (2001).
7. L. B. Ioffe, V. B. Geshkenbein, M. V. Feigel'man, A. L. Fauchère, G. Blatter, Environmentally decoupled sds -wave Josephson junctions for quantum computing. *Nature* **398**, 679 (1999).
8. J. E. Mooij, T. P. Orlando, L. Levitov, L. Tian, C. H. van der Wal, S. Lloyd, Josephson Persistent-Current Qubit. *Science* **285**, 1036 (1999).

9. T. Yamashita, K. Tanikawa, S. Takahashi, S. Maekawa, Superconducting π Qubit with a Ferromagnetic Josephson Junction. *Phys. Rev. Lett.* **95**, 097001 (2005).
10. T. Kontos, M. Aprili, J. Lesueur, F. Genêt, B. Stephanidis, R. Boursier, Josephson Junction through a Thin Ferromagnetic Layer: Negative Coupling. *Phys. Rev. Lett.* **89**, 137007 (2002).
11. J. W. A. Robinson, S. Piano, G. Burnell, C. Bell, M. G. Blamire, Critical Current Oscillations in Strong Ferromagnetic π Junctions. *Phys. Rev. Lett.* **97**, 177003 (2006).
12. M. Weides, M. Kemmler, H. Kohlstedt, R. Waser, D. Koelle, R. Kleiner, E. Goldobin, $0-\pi$ Josephson Tunnel Junctions with Ferromagnetic Barrier. *Phys. Rev. Lett.* **97**, 247001 (2006).
13. C. Bell, R. Loloee, G. Burnell, M. G. Blamire, Characteristics of strong ferromagnetic Josephson junctions with epitaxial barriers. *Phys. Rev. B* **71**, 180501 (2005).
14. V. V. Ryazanov, V. A. Oboznov, A. Y. Rusanov, A. V. Veretennikov, A. A. Golubov, J. Aarts, Coupling of Two Superconductors through a Ferromagnet: Evidence for a π Junction. *Phys. Rev. Lett.* **86**, 2427-2430 (2001).
15. Y. Blum, A. Tsukernik, M. Karpovski, A. Palevski, Oscillations of the Superconducting Critical Current in Nb-Cu-Ni-Cu-Nb Junctions. *Phys. Rev. Lett.* **89**, 187004 (2002).
16. V. Shelukhin, A. Tsukernik, M. Karpovski, Y. Blum, K. B. Efetov, A. F. Volkov, T. Champel, M. Eschrig, T. Löfwander, G. Schön, A. Palevski, Observation of periodic π-phase shifts in ferromagnet-superconductor multilayers. *Phys. Rev. B* **73**, 174506 (2006).
17. J. W. A. Robinson, S. Piano, G. Burnell, C. Bell, M. G. Blamire, Zero to π transition in superconductor-ferromagnet-superconductor junctions. *Phys. Rev. B* **76**, 094522 (2007).
18. W. Han, S. Maekawa, X.-C. Xie, Spin current as a probe of quantum materials. *Nat. Mater.* **19**, 139–152 (2020).
19. R. H. Silsbee, A. Janossy, P. Monod, Coupling between ferromagnetic and conduction-spin-resonance modes at a ferromagnetic\normal-metal interface. *Phys. Rev. B* **19**, 4382-4399 (1979).
20. Y. Tserkovnyak, A. Brataas, G. E. W. Bauer, B. I. Halperin, Nonlocal magnetization dynamics in ferromagnetic heterostructures. *Rev. Mod. Phys.* **77**, 1375-1421 (2005).
21. L. Landau, E. Lifshitz, On the theory of the dispersion of magnetic permeability in ferromagnetic bodies. *Phys. Z. Sowjetunion* **8**, 153 (1935).
22. T. L. Gilbert, A phenomenological theory of damping in ferromagnetic materials. *Magnetics, IEEE Transactions on* **40**, 3443-3449 (2004).
23. J. C. Slonczewski, Current-driven excitation of magnetic multilayers. *J. Magn. Magn. Mater.* **159**, L1-L7 (1996).
24. C. Bell, S. Milikisyants, M. Huber, J. Aarts, Spin Dynamics in a Superconductor-Ferromagnet Proximity System. *Phys. Rev. Lett.* **100**, 047002 (2008).
25. J. P. Morten, A. Brataas, G. E. W. Bauer, W. Belzig, Y. Tserkovnyak, Proximity-effect–assisted decay of spin currents in superconductors. *Europhys. Lett.* **84**, 57008 (2008).
26. C. Holmqvist, S. Teber, M. Fogelström, Nonequilibrium effects in a Josephson junction coupled to a precessing spin. *Phys. Rev. B* **83**, 104521 (2011).
27. M. Inoue, M. Ichioka, H. Adachi, Spin pumping into superconductors: A new probe of spin dynamics in a superconducting thin film. *Phys. Rev. B* **96**, 024414 (2017).
28. Y. Yao, Q. Song, Y. Takamura, J. P. Cascales, W. Yuan, Y. Ma, Y. Yun, X. C. Xie, J. S. Moodera, W. Han, Probe of spin dynamics in superconducting NbN thin films via spin pumping. *Phys. Rev. B* **97**, 224414 (2018).

29. K.-R. Jeon, C. Ciccarelli, A. J. Ferguson, H. Kurebayashi, L. F. Cohen, X. Montiel, M. Eschrig, J. W. A. Robinson, M. G. Blamire, Enhanced spin pumping into superconductors provides evidence for superconducting pure spin currents. *Nat. Mater.* **17**, 499–503 (2018).
30. J. A. Sauls, Andreev bound states and their signatures. *Philos. Trans. Royal Soc. A* **376**, 20180140 (2018).
31. M. Eschrig, Theory of Andreev bound states in S-F-S junctions and S-F proximity devices. *Phil. Trans. R. Soc. A* **376**, 20150149 (2018).
32. S. S. P. Parkin, N. More, K. P. Roche, Oscillations in exchange coupling and magnetoresistance in metallic superlattice structures: Co/Ru, Co/Cr, and Fe/Cr. *Phys. Rev. Lett.* **64**, 2304-2307 (1990).
33. D. L. Mills, Ferromagnetic resonance relaxation in ultrathin metal films: The role of the conduction electrons. *Phys. Rev. B* **68**, 014419 (2003).
34. T. Wakamura, H. Akaike, Y. Omori, Y. Niimi, S. Takahashi, A. Fujimaki, S. Maekawa, Y. Otani, Quasiparticle-mediated spin Hall effect in a superconductor. *Nat. Mater.* **14**, 675-678 (2015).
35. M. Eschrig, T. Löfwander, Triplet supercurrents in clean and disordered half-metallic ferromagnets. *Nat. Phys.* **4**, 138 (2008).
36. M. Houzet, Ferromagnetic Josephson Junction with Precessing Magnetization. *Phys. Rev. Lett.* **101**, 057009 (2008).
37. C. W. J. Beenakker, Universal limit of critical-current fluctuations in mesoscopic Josephson junctions. *Phys. Rev. Lett.* **67**, 3836-3839 (1991).
38. A. A. Golubov, M. Y. Kupriyanov, E. Il'ichev, The current-phase relation in Josephson junctions. *Rev. Mod. Phys.* **76**, 411-469 (2004).
39. T. Wakamura, N. Hasegawa, K. Ohnishi, Y. Niimi, Y. Otani, Spin Injection into a Superconductor with Strong Spin-Orbit Coupling. *Phys. Rev. Lett.* **112**, 036602 (2014).
40. C. Chappert, K. L. Dang, P. Beauvillain, H. Hurdequint, D. Renard, Ferromagnetic resonance studies of very thin cobalt films on a gold substrate. *Phys. Rev. B* **34**, 3192-3197 (1986).
41. W. Platow, A. N. Anisimov, G. L. Dunifer, M. Farle, K. Baberschke, Correlations between ferromagnetic-resonance linewidths and sample quality in the study of metallic ultrathin films. *Phys. Rev. B* **58**, 5611-5621 (1998).
42. Y. Zhao, Q. Song, S.-H. Yang, T. Su, W. Yuan, S. S. P. Parkin, J. Shi, W. Han, Experimental Investigation of Temperature-Dependent Gilbert Damping in Permalloy Thin Films. *Scientific Reports* **6**, 22890 (2016).
43. K.-R. Jeon, C. Ciccarelli, H. Kurebayashi, L. F. Cohen, X. Montiel, M. Eschrig, T. Wagner, S. Komori, A. Srivastava, J. W. A. Robinson, M. G. Blamire, Effect of Meissner Screening and Trapped Magnetic Flux on Magnetization Dynamics in Thick Nb/$Ni_{80}Fe_{20}$/Nb Trilayers. *Phys. Rev. Appl.* **11**, 014061 (2019).
44. Y. Tserkovnyak, A. Brataas, G. E. W. Bauer, Enhanced Gilbert Damping in Thin Ferromagnetic Films. *Phys. Rev. Lett.* **88**, 117601 (2002).
45. H. J. Skadsem, A. Brataas, J. Martinek, Y. Tserkovnyak, Ferromagnetic resonance and voltage-induced transport in normal metal-ferromagnet-superconductor trilayers. *Phys. Rev. B* **84**, 104420 (2011).
46. T. Yu, G. E. W. Bauer, Noncontact Spin Pumping by Microwave Evanescent Fields. *Phys. Rev. Lett.* **124**, 236801 (2020).

47. M. T. Ahari, Y. Tserkovnyak, Superconductivity-enhanced spin pumping: The role of Andreev bound-state resonances. *arXiv:2009.04423*, (2020).
48. A. F. Andreev, The Thermal Conductivity of the Intermediate State in Superconductors. *JETP* **19**, 1228 (1964).
49. P. Townsend, J. Sutton, Investigation by Electron Tunneling of the Superconducting Energy Gaps in Nb, Ta, Sn, and Pb. *Phys. Rev.* **128**, 591-595 (1962).
50. A. V. Pronin, M. Dressel, A. Pimenov, A. Loidl, I. V. Roshchin, L. H. Greene, Direct observation of the superconducting energy gap developing in the conductivity spectra of niobium. *Phys. Rev. B* **57**, 14416-14421 (1998).
51. J. Bass, W. P. Pratt, Spin-diffusion lengths in metals and alloys, and spin-flipping at metal/metal interfaces: an experimentalist's critical review. *J. Phys. Condens. Matter.* **19**, 183201 (2007).
52. A. A. Bannykh, J. Pfeiffer, V. S. Stolyarov, I. E. Batov, V. V. Ryazanov, M. Weides, Josephson tunnel junctions with a strong ferromagnetic interlayer. *Phys. Rev. B* **79**, 054501 (2009).

Acknowledgments

General: We acknowledge the fruitful discussion with Ziqiang Qiu, Zhe Yuan, Ke Xia, Young Sun, and Kei Yamamoto. Y.Y., R.C., Y.M., W.X., Y.J., X.C.X., and W.H. acknowledge the financial support from National Basic Research Programs of China (No. 2019YFA0308401), National Natural Science Foundation of China (No. 11974025), Beijing Natural Science Foundation (No. 1192009), and the Strategic Priority Research Program of the Chinese Academy of Sciences (No. XDB28000000). T.Y. is financially supported by DFG Emmy Noether program (SE 2558/2-1). Y.T. and S.M. acknowledge the financial support from ERATO- JST (JPMJER1402), and KAKENHI (No. 26103005, No. JP16H04023, and No. JP26247063) from MEXT, Japan.

Author contributions: W.H. conceived and supervised the project. Y.Y. and R.C. performed the ferromagnetic resonance measurements. Y.Y. and Y.M. performed X-ray diffraction measurements. T.Y., Y.T., and S.M. performed the theoretical calculations. S.H.Y. synthesized the Nb/NiFe/Nb heterostructures. Y.Y. and W.H. wrote the manuscript with the contribution from all authors. All the authors discussed the results.

Competing interests: The authors declare no competing interests.

Data Availability: All data needed to evaluate the conclusions in the paper are present in the paper and/or the Supplementary Materials. Additional data related to this paper may be requested from the authors.

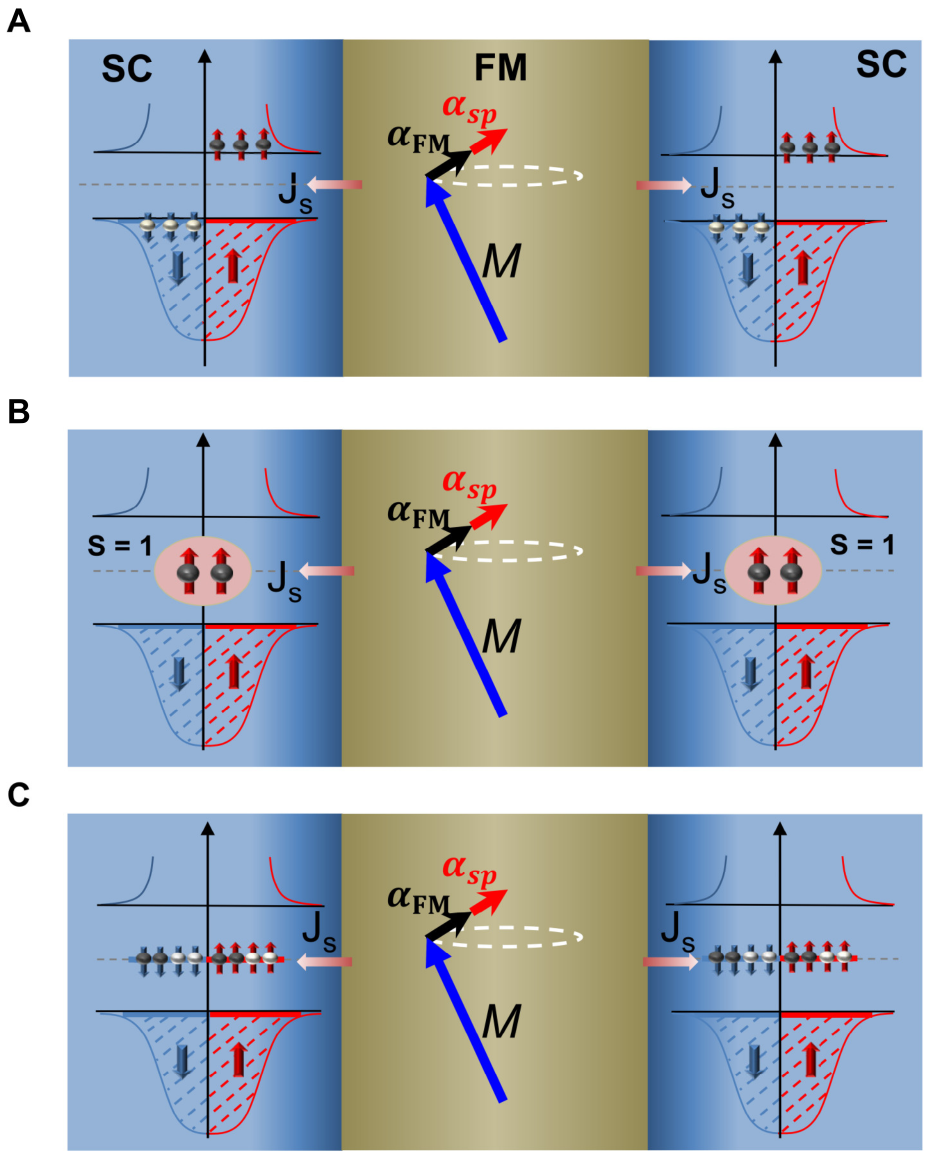

s

Fig. 1. Illustration of magnetization dynamics and spin pumping in the SC/FM/SC heterostructures. (**A-C**) Spin pumping and enhanced Gilbert damping in the SC/FM/SC heterostructures with spin current (J_S) in SC layers that can be mediated by Bogoliubov quasiparticles (**A**, indicated by the spin-polarized electron-/hole-like quasiparticles above the superconducting gap edge), the equal spin-triplet Cooper pairs (**B**), and the zero-energy ABS (**C**). $\boldsymbol{M}$ and α_{FM} are the magnetization and Gilbert damping of the FM layer itself, and α_{sp} is the enhanced Gilbert damping, which arises from the spin dissipation in SC layers during the spin pumping process.

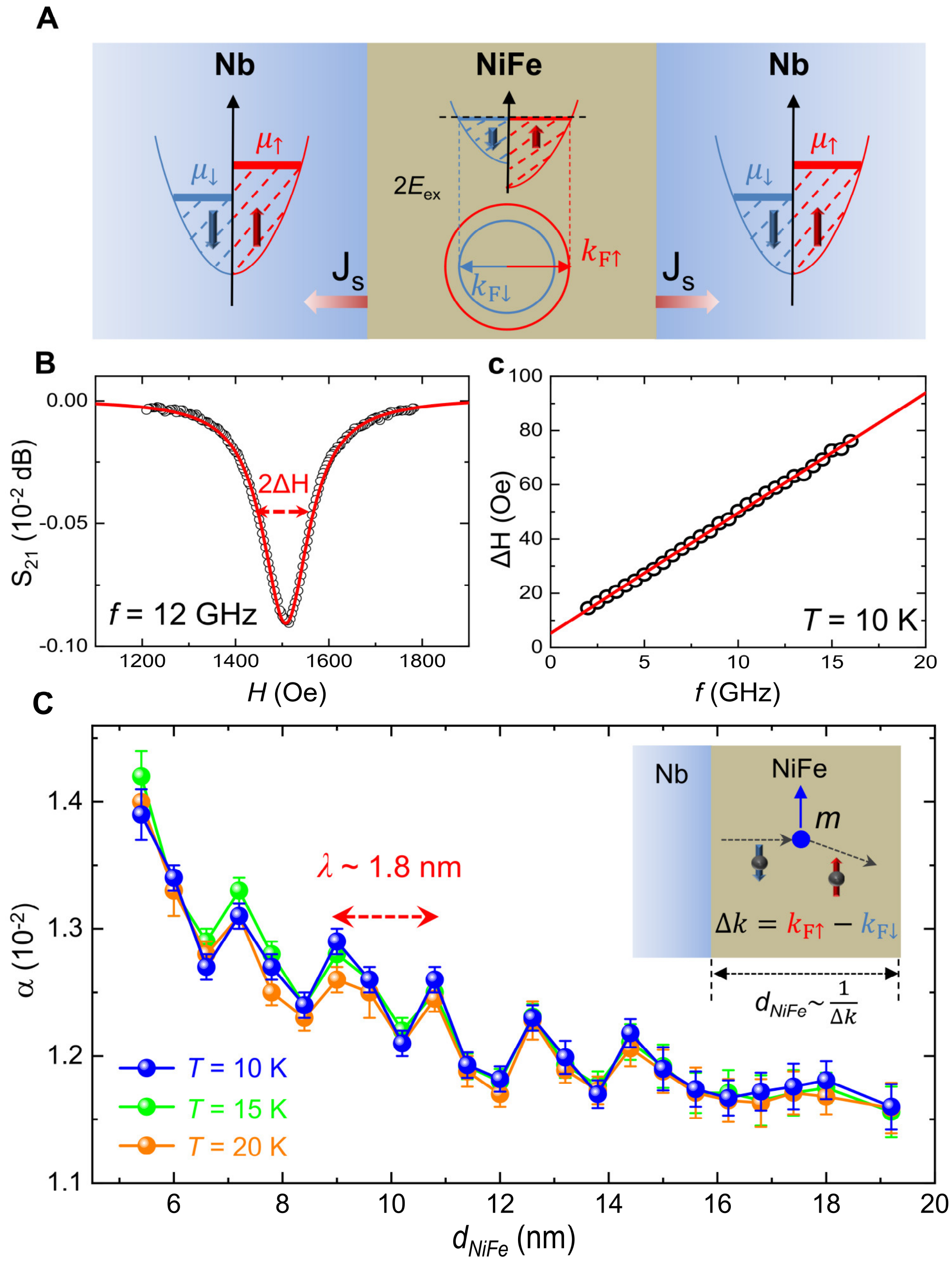

Fig. 2. Oscillatory Gilbert damping of the Nb/NiFe/Nb heterostructures above T_C. (**A**) The illustration of spin pumping into the normal states of Nb layers and the electronic band structure of NiFe with different spin-up and spin-down Fermi vectors ($k_{F\uparrow}$ and $k_{F\downarrow}$) due to the exchange splitting ($2E_{ex}$). The spin pumping gives rise to the spin accumulation in the Nb layers, indicated by the spin-split chemical potential ($\mu_\uparrow$ and $\mu_\downarrow$). (**B**) A typical FMR curve measured with f = 12 GHz (black circles) and the Lorentzian fitting curve (red line) measured on Nb/Py (12 nm)/Nb. ΔH is the half linewidth at the half maximum of FMR signal. (**C**) The determination of the Gilbert

damping from ΔH vs. *f*. The red line represents the best linear-fitting curve. (**D**) The oscillatory Gilbert damping as a function of NiFe thickness (d_{NiFe}) measured at T = 10, 15, and 20 K, respectively. The experimental oscillating period (λ) is marked by the red dashed arrow. The inset: Illustration of the quantum-interference effect of the angular momentum transfer between the local magnetic moment and the spin-polarized electrons when the NiFe thickness decreases to the length scale of $1/\Delta k$.

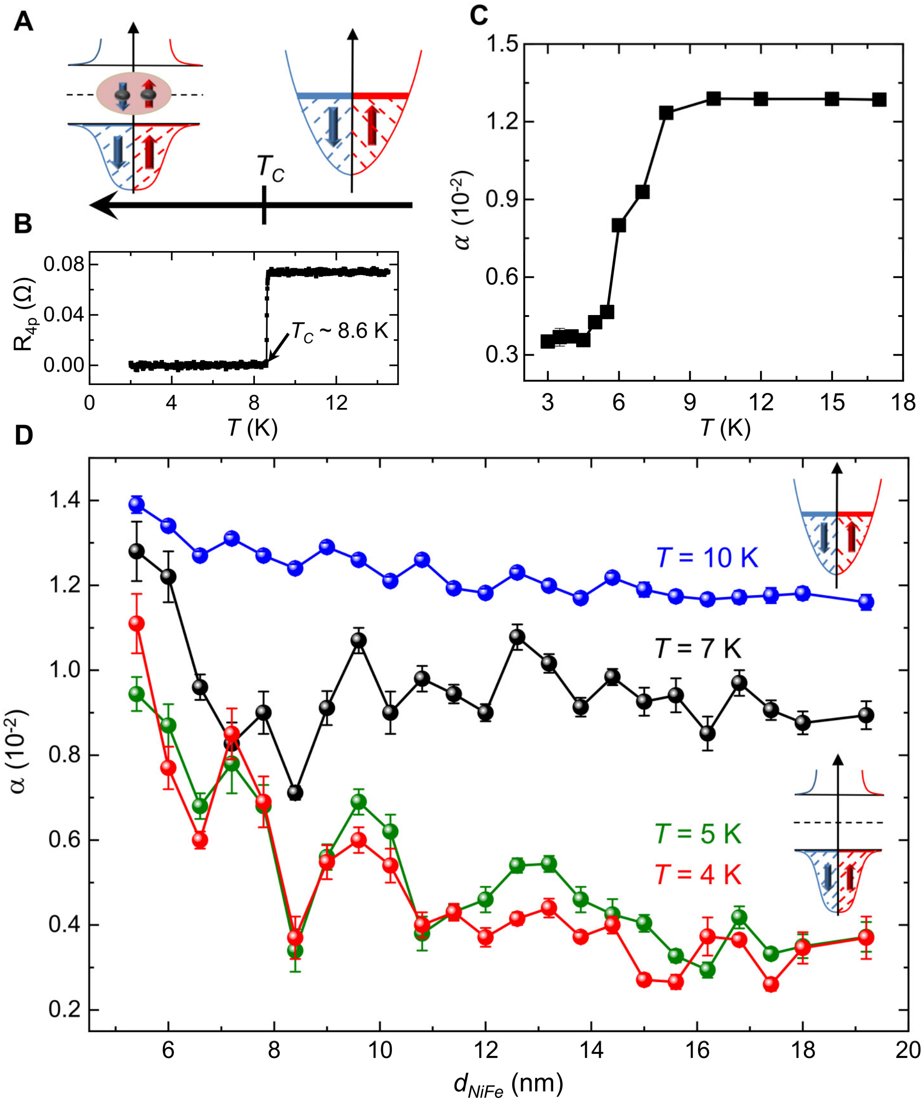

Fig. 3. Giant oscillatory Gilbert damping in Nb/NiFe/Nb heterostructures below T_C. (**A**) The illustration of electronic band structures of Nb in the normal and superconducting states. (**B**) The determination of T_C via zero-resistance temperature measured on the typical Nb/NiFe (12 nm)/Nb heterostructures. (**C**) Temperature dependence of Gilbert damping of the typical Nb/NiFe (12 nm)/Nb heterostructures. (**D**) The oscillatory Gilbert damping as a function of the NiFe thickness in the Nb/NiFe/Nb heterostructures measured at T = 10, 7, 5, and 4 K, respectively. The oscillating feature below T_C (T = 4 and 5 K) is dramatically enhanced compared to that above T_C (T = 10 K).

A

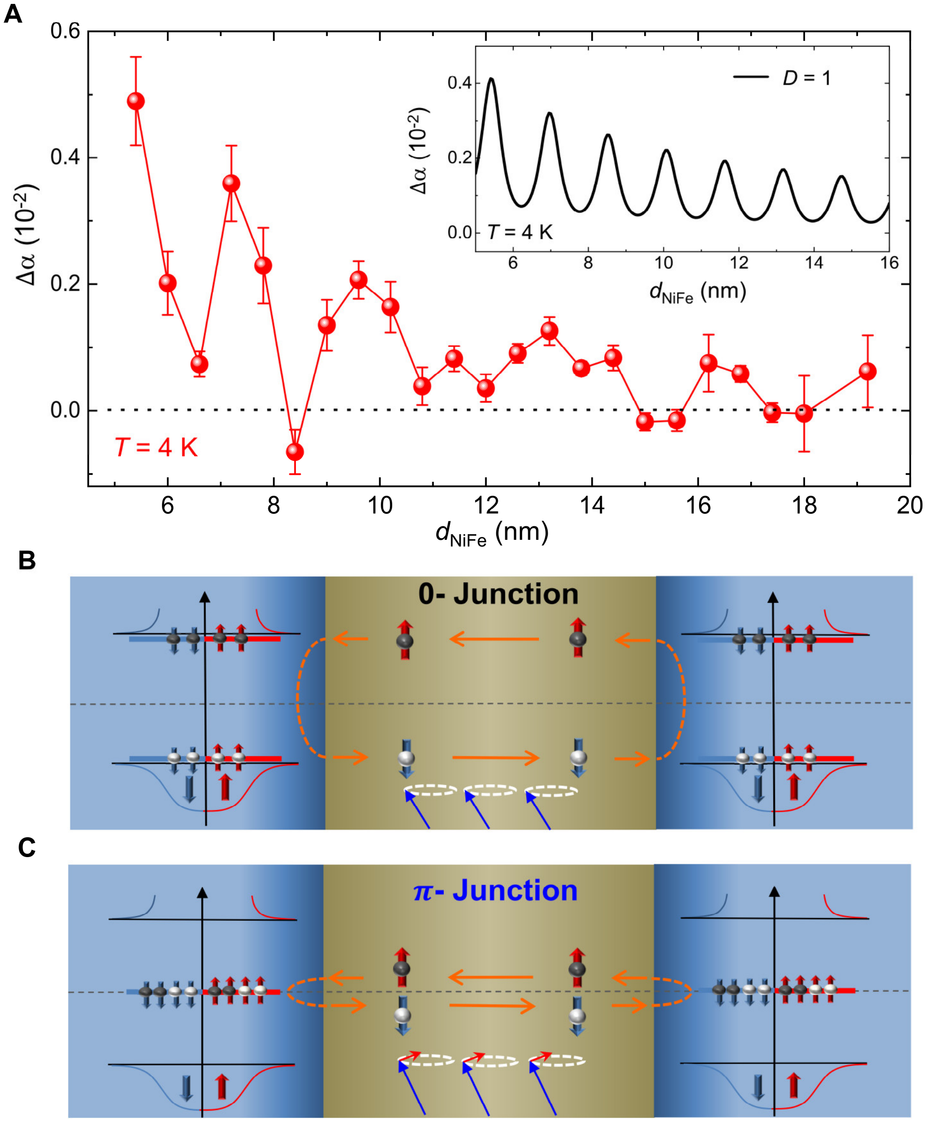

Fig. 4. Physical mechanism of the giant oscillatory Gilbert damping in Nb/NiFe/Nb junctions. (**A**) The NiFe thickness dependence of the Gilbert damping difference (Δα) between the Nb/NiFe/Nb π- and *zero*-junctions. Inset: The calculated damping difference between the *zero*- and π-junctions as a result of spin pumping into ABS inside the superconducting gaps. (**B-C**) Illustration of the spin pumping via the ABS and the enhanced Gilbert damping for Nb/NiFe/Nb *zero*- and π-junctions, respectively. For *zero*-junctions (**B**), the ABS are close to the superconducting gap edge. While for π-junctions (**C**), the ABS are around the zero-energy. The white and darkgray balls represent the hole-like and electron-like Andreev particles.

Supplementary Materials for

Giant oscillatory Gilbert damping in superconductor/ferromagnet/superconductor junctions

Authors

Yunyan Yao[1,2†], Ranran Cai[1,2†], Tao Yu[3], Yasumasa Tsutsumi[4], Yang Ma[1,2], Wenyu Xing[1,2], Yuan Ji[1,2], Xin-Cheng Xie[1,2,5,6], See-Hun Yang[7]*, Sadamichi Maekawa[4,8]*, and Wei Han[1,2]*

This file includes:

- Supplementary Materials and Methods
- fig. S1. The crystalline properties of the Nb/NiFe/Nb heterostructures.
- fig. S2. Gilbert damping measurement of Nb/NiFe/Nb heterostructures at T = 10 K.
- fig. S3. NiFe thickness dependence of T_C for the Nb/NiFe/Nb heterostructures.
- fig. S4. Measurement of the Gilbert damping of Nb/NiFe/Nb heterostructures at T = 4 K.
- fig. S5. The effect of FMR measurement on the T_C of Nb/NiFe/Nb heterostructures.
- fig. S6. The Gilbert damping of *zero*- and π-junctions at T = 4 K.
- fig. S7. The measurement of Josephson coupling in Nb/NiFe/Nb junctions.
- fig. S8. Calculation of the enhanced Gilbert damping due to spin pumping via the ABS at T = 4 K.
- fig. S9. Gilbert damping of control sample of bilayer Nb/NiFe junctions.

Supplementary Materials

Section 1: Model of oscillating Gilbert damping above T_C.

The oscillatory Gilbert damping in normal metal (NM)/ferromagnet (FM)/NM heterostructures arising from quantum interference effect is analyzed based on previous theory by Mills (*33*). Within the linear response theory, the enhanced Gilbert damping is related to the dynamical spin susceptibility ($\chi^{-+}(\Omega)$) of conduction electrons in a FM,

$$\alpha_{\mathrm{sp}} = \frac{J^2 M_s V}{2N^2\hbar^3\gamma}\Lambda_2 \tag{S1}$$

where $\Lambda_2 = \mathrm{Im}\left(\left.\frac{d\chi^{-+}(\Omega)}{d\Omega}\right|_{\Omega=0}\right)$. Using one dimensional model, we obtain

$$\Lambda_2 = \frac{1}{\pi^2}\int_{\mathrm{FM}} dxdx' \mathrm{Im}[G_\uparrow(x,x',\epsilon_{\mathrm{F}})]\mathrm{Im}[G_\downarrow(x,x',\epsilon_{\mathrm{F}})] \tag{S2}$$

where $G_\sigma(x,x',\epsilon_{\mathrm{F}})$ is the Green's function for conduction electrons with σ-spin at the Fermi energy (ϵ_{F}). In a FM, $G_\sigma(x,x',\epsilon_{\mathrm{F}})$ is related to the exchange energy.

$$\left[-\frac{\hbar^2}{2m}\frac{d}{dx^2} - \epsilon \pm E_{\mathrm{ex}}\right]G_\sigma(x,x',\epsilon_{\mathrm{F}}) = \delta(x-x') \tag{S3}$$

For the FM film with a thickness d_{FM} in $-d_{\mathrm{FM}}/2 < x < d_{\mathrm{FM}}/2$, the Green's function satisfies the relation

$$G_\sigma(x,x',\epsilon_{\mathrm{F}}) = G_\sigma(x',x,\epsilon_{\mathrm{F}}) = G_\sigma(-x,-x',\epsilon_{\mathrm{F}}) \tag{S4}$$

Hence, the imaginary part of the Green's function could be expressed by

$$\mathrm{Im}[G_\sigma(x,x',\epsilon_{\mathrm{F}})] = -\pi\{N_{\mathrm{F}\sigma}\cos[k_{\mathrm{F}\sigma}(x-x')] + N'_{\mathrm{F}\sigma}\cos[k_{\mathrm{F}\sigma}(x+x')]\} \tag{S5}$$

where $k_{\mathrm{F}\sigma} = \sqrt{\frac{2m}{\hbar^2}(\epsilon_{\mathrm{F}} \mp E_{\mathrm{ex}})}$ is the Fermi wave-vector in the FM, $N_{\mathrm{F}\sigma}$ and $N'_{\mathrm{F}\sigma}$ are equivalent to the density of states and the modulation amplitude of the local density of states, respectively. For the same position of x, the local density of states is equal to

$$N_\sigma(x,\epsilon_{\mathrm{F}}) = N_{\mathrm{F}\sigma} + N'_{\mathrm{F}\sigma}\cos[2k_{\mathrm{F}\sigma}x] \tag{S6}$$

Since E_{ex} is much smaller compared to ϵ_{F}, the spatial modulation of the local density of states is negligible. The combination of equations (S2) and (S5) leads to

$$\Lambda_2 = \int_{-d_{\mathrm{FM}}/2}^{d_{\mathrm{FM}}/2} dxdx' \{N_{\mathrm{F}\uparrow}\cos[k_{\mathrm{F}\uparrow}(x-x')]\} * \{N_{\mathrm{F}\downarrow}\cos[k_{\mathrm{F}\downarrow}(x-x')]\} \tag{S7}$$

$$= 2N_{\mathrm{F}\uparrow}N_{\mathrm{F}\downarrow}\left\{\frac{1}{(k_{\mathrm{F}\uparrow}-k_{\mathrm{F}\downarrow})^2}\sin^2\left[\frac{k_{\mathrm{F}\uparrow}-k_{\mathrm{F}\downarrow}}{2}d_{\mathrm{FM}}\right]+\frac{1}{(k_{\mathrm{F}\uparrow}+k_{\mathrm{F}\downarrow})^2}\sin^2\left[\frac{k_{\mathrm{F}\uparrow}+k_{\mathrm{F}\downarrow}}{2}d_{\mathrm{FM}}\right]\right\}$$

Clearly, the enhanced Gilbert damping is expected to oscillate as a function of the FM thickness with two periods of $2\pi/[k_{\mathrm{F}\uparrow}-k_{\mathrm{F}\downarrow}]$ and $2\pi/[k_{\mathrm{F}\uparrow}+k_{\mathrm{F}\downarrow}]$. For real FM materials, such as NiFe with $(k_{\mathrm{F}\uparrow}+k_{\mathrm{F}\downarrow}) \gg (k_{\mathrm{F}\uparrow}-k_{\mathrm{F}\downarrow})$, the second term in the equation (S7) could be negligible, leaving only one oscillating period of $2\pi/[k_{\mathrm{F}\uparrow}-k_{\mathrm{F}\downarrow}]$. When the FM thickness is equal to $2n\pi/[k_{\mathrm{F}\uparrow}-k_{\mathrm{F}\downarrow}]$, a lower Gilbert damping is obtained. On the other hand with FM thickness of $(2n+1)\pi/[k_{\mathrm{F}\uparrow}-k_{\mathrm{F}\downarrow}]$, a larger Gilbert damping is obtained.

Section 2: Calculation of the enhanced Gilbert damping in Nb/NiFe/Nb by spin pumping via Andreev bound states (ABS).

As the reciprocal process of the spin transfer torque, conventional spin pumping is achieved by the magnetization torques provided by the driven quasiparticle carriers (*20, 44-46*), which are the electrons in the normal metals. In SC/FM heterostructures, however, the quasiparticle carriers can be either Bogoliubov quasiparticles or ABS (*37*), which lie above and within the superconducting gaps, respectively. Therefore, it is desirable to formulate and estimate the contribution to the spin pumping via the ABS (*47*), when the temperature is much smaller than the superconducting critical temperature.

Without loss of generality, we start the analysis from a left-propagating electron of energy ε and spin $\sigma = \{\uparrow, \downarrow\} = \{+, -,\}$. When the Zeeman splitting J is much smaller than the Fermi energy E_F, it has momentum

$$k_\sigma = k_F + (\varepsilon + \sigma J)/(\hbar \nu_F), \tag{S8}$$

where ν_F is the Fermi velocity of the electrons. When one electron goes from the FM to the SCs, it is reflected as a hole by the Andreev reflection at the right FM/SC interface; this hole has a phase shift $\chi = -\arccos(\varepsilon/\Delta)$ with respect to the electron (*48*), where Δ is the superconducting gap. Similarly, when a hole goes from the metal to the superconductor at the left FM/SC interface, an electron can be reflected. With a proper energy, the Andreev reflections can form a closed path, as a result of which the ABS forms. This requires that the phase accumulated in the reflections satisfies the Sommerfeld quantization condition, i.e. in the ballistic regime,

$$\frac{\varepsilon L}{\hbar v_F} + \sigma\frac{Jd_{\mathrm{NiFe}}}{\hbar v_F} - \arccos\left(\frac{\varepsilon}{\Delta}\right) = n\pi, \tag{S9}$$

where d_{NiFe} is the thickness of the FM layer and n is an integer. Since $\hbar v_F/\Delta \geq 100$ nm with $v_F = 2.2 \times 10^5$ m/s and $\Delta = 1$ meV at $T = 4$ K in our experiment (*17, 49, 50*), $d_{\mathrm{NiFe}} < 19$ nm $<< \hbar v_F/\Delta$ such that the first term in Eq. (S9) can be safely disregarded. Hence, the energy of the ABS can be described by $\varepsilon = \pm\Delta\cos(\frac{Jd_{\mathrm{NiFe}}}{\hbar v_F})$ for ideal case without any scattering. In reality, the interfacial scattering need to be taken into account. Following Beenakker[6], an interfacial transmission coefficient is introduced to include the interfacial scattering and the diffusive regime in the dirty limit, the energy of the ABS reads,

$$\varepsilon_0 = \pm\Delta\sqrt{1 - D\sin^2\left(\frac{Jd_{\mathrm{NiFe}}}{\hbar v_F}\right)}, \tag{S10}$$

where D is the transmission coefficient at the interface, which is close to 1 in the ballistic regime (mean free path $l > d_{\mathrm{NiFe}}$), and close to 0 for the long diffusive regime ($l << d_{\mathrm{NiFe}}$). The energy of the ABS oscillates from the edge of the superconducting gap to the zero-energy with the variation of the FM thickness (fig. S8A). The calculation of spin pumping through ABS at finite temperature is straightforward following Refs. 4 and 7. The pumped spin current reads (*20, 44-46*),

$$\mathbf{J}_s(t) = \frac{\hbar}{4\pi} g_{\mathrm{eff}}^{\uparrow\downarrow} \boldsymbol{m} \times \frac{d\boldsymbol{m}}{dt}, \tag{S11}$$

where $\boldsymbol{m}$ is the magnetization unit vector, and we define the effective mixing spin conductivity $g_{\mathrm{eff}}^{\uparrow\downarrow}$ at the finite temperature via the zero-temperature one $g^{\uparrow\downarrow}$ by (*45, 47*)

$$g_{\mathrm{eff}}^{\uparrow\downarrow} = n_0 \int d\varepsilon \frac{df(\varepsilon)}{d\varepsilon} \mathrm{Re}[g^{\uparrow\downarrow}(\varepsilon)]. \tag{S12}$$

Here, n_0 is the number of the conduction channel that roughly corresponds the conduction electron density at the interface and $f(\varepsilon) = 1/\{\exp[\varepsilon/(k_B T)] + 1\}$ is the Fermi-Dirac distribution of electron at the temperature T. Importantly, in the ballistic limit $\mathrm{Re}[g^{\uparrow\downarrow}(\varepsilon)] = 1$ when $\varepsilon = \varepsilon_0$; it has width $\Delta\varepsilon$ depending on the FM thickness d_{NiFe} in the ballistic regime or the mean free path l_m in the diffusive regime. By the uncertainty principle, $\Delta\varepsilon\Delta t = 2\pi\hbar$, where $\Delta t = l_m/v_F$ is the propagation time of the electron in the junction, leading to $\Delta\varepsilon \sim 2\pi\hbar v_F/l_m$. By further considering the degeneracy due to spin (×2) and particle-hole (×2) symmetries and the existence of two interfaces (×2), we thus can estimate

$$g_{\mathrm{eff}}^{\uparrow\downarrow} \sim 16\pi n_0 \frac{\hbar v_F}{l_m} \frac{df(\varepsilon_0)}{d\varepsilon}. \tag{S13}$$

The pumped spin current carries the angular momentum away from the precessing magnetization and hence cause an enhanced Gilbert damping, which is described by

$$\delta\alpha = 4 n_0 \gamma \frac{\hbar^2 v_F}{M_s l_m d_{\mathrm{NiFe}}} \frac{df(\varepsilon_0)}{d\varepsilon}, \tag{S14}$$

where γ is electron gyromagnetic ratio and M_s is the saturated magnetization of the ferromagnet.

We are now ready to estimate the contribution of ABS to the Gilbert damping at $T = 4$ K with varying transmission coefficient. We take $n_0 = 0.5 \times 10^{16}$ m^{-2} following Ref. 2, $l_m \sim 3$ nm, $v_F = 2.2 \times 10^5$ m/s, $J = 400$ meV and $\mu_0 M_s \approx 1\,T$ from previous experimental results (*17*). With superconducting gaps $\Delta \approx 1$ meV at $T = 4$ K for Nb (*49, 50*), Figure S8A plots the normalized energy of ABS by the superconducting gap at $T = 4$ K as a function of d_{NiFe} with $D = 1.0$, 0.8, and 0.6, and 0.4, respectively. Figure S8B shows the additional Gilbert damping contributed by spin pumping to the ABS with $D = 1.0$, 0.8, 0.6, and 0.4, respectively. For simplicity, we have disregarded the possible thickness dependence of the superconducting gaps and magnetizations. As the transmission coefficient D decrease from 1.0 to 0.4, the energy of ABS related to the π-junctions increase, leading to the decrease of the additional Gilbert damping. Our minimal theoretical estimation demonstrates that large oscillating Gilbert damping can be still resolved with D in the range from 0.4 to 1.0 (fig. S8B). To be noted, our theoretical estimation is based on a simplified model that assumes D does not depend on the NiFe thickness. In reality, D decreases as the NiFe thickness increases from the ballistic regime to the dirty/diffusive regime. Further theoretical studies are needed to quantitatively investigate the experimental data.

Section 3: Measurement of the Josephson coupling in Nb/NiFe/Nb.

The Nb/NiFe/Nb Josephson devices are fabricated using the shadow mask techniques during the films growth. As shown in figs. S7A and S7B, the Josephson devices have a junction area (A) of ~ 80 µm × 80 µm, and the other areas are electrically isolated by a 100 nm AlO_x layer. The Josephson current is measured by standard a.c. lock-in technique. The normalized differential resistances (dV/dI) measured on the Nb/NiFe (5 nm)/Nb junction at various temperatures are shown in fig. S7C. The critical current (I_c) is defined as point where the differential resistance increases above the value for the zero-bias current. The normal resistance (R_n) is determined to be the saturated value of the normal states of the Josephson coupling measurement. The measured area-resistance product (R_nA) of $\sim 5 \times 10^{-10}\ \Omega m^2$ is higher than that reported in metallic Josephson junction (*17, 51*), and comparable to that of FM Josephson junction with a thin tunnel barrier (*52*). This behavior indicates that there is most likely a thin $NiFeO_x$ layer (indicated by Fig. S7b) in the junction formed during the AlO_x growth step in the presence of oxygen gas. As the temperature increases, I_c and the characteristic voltage (I_cR_n) decrease (figs. S7C and S7D). Clear Josephson currents are observed on the Nb/NiFe (5 nm)/Nb junction and Nb/NiFe (10 nm)/Nb junction (figs. S7E and S7F). On the other hand, no Josephson current could be observed in the Nb/NiFe (30 nm)/Nb junction (figs. S7E and S7F). The absence of Josephson current in Nb/NiFe (30 nm)/Nb junction indicates that there is no long-range spin-triplet Josephson coupling in the Nb/NiFe/Nb heterostructures in our experiment.

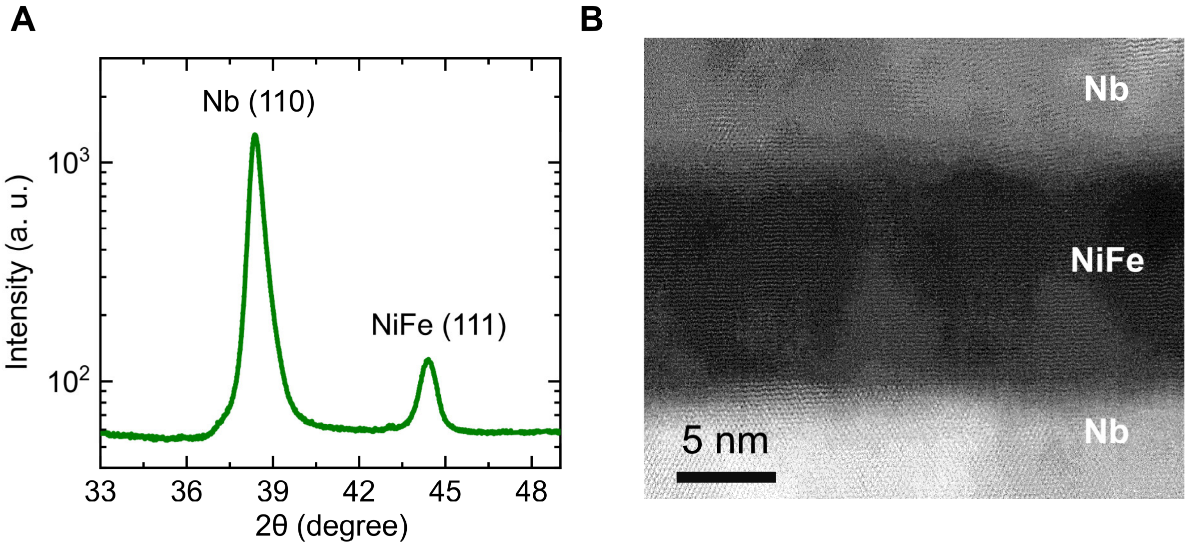

fig. S1. The crystalline properties of the Nb/NiFe/Nb heterostructures. (**A**) The θ-2θ X-ray diffraction results measured on the typical Nb/NiFe (12 nm)/Nb sample, where Nb (110) and NiFe (111) peaks are observed. (**B**) High-resolution transmission electron micrographs measured on the typical Nb/NiFe (12 nm)/Nb sample.

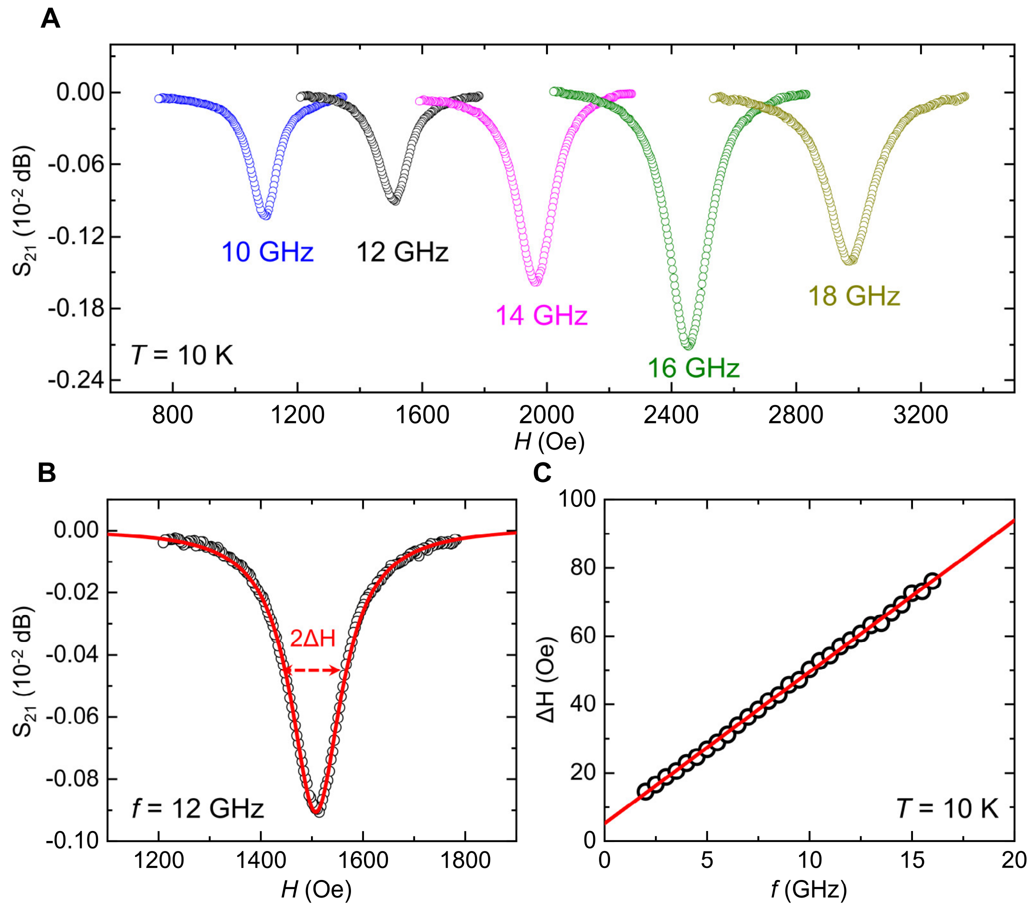

fig. S2. Gilbert damping measurement of Nb/NiFe/Nb heterostructures at *T* = 10 K. (**A**) The typical FMR spectra as a function of magnetic field with microwave frequency (*f*) of 10, 12, 14, 16, and 18 GHz, respectively. (**B**) The typical FMR spectrum measured with *f* = 12 GHz (black circles) and the Lorentz fitting curve (red line). ΔH is the half linewidth of the FMR signal. (**C**) The determination of the Gilbert damping from ΔH vs. *f*. The red line indicates the best linear-fitting curve. These results are obtained on the typical Nb/Py (12 nm)/Nb sample.

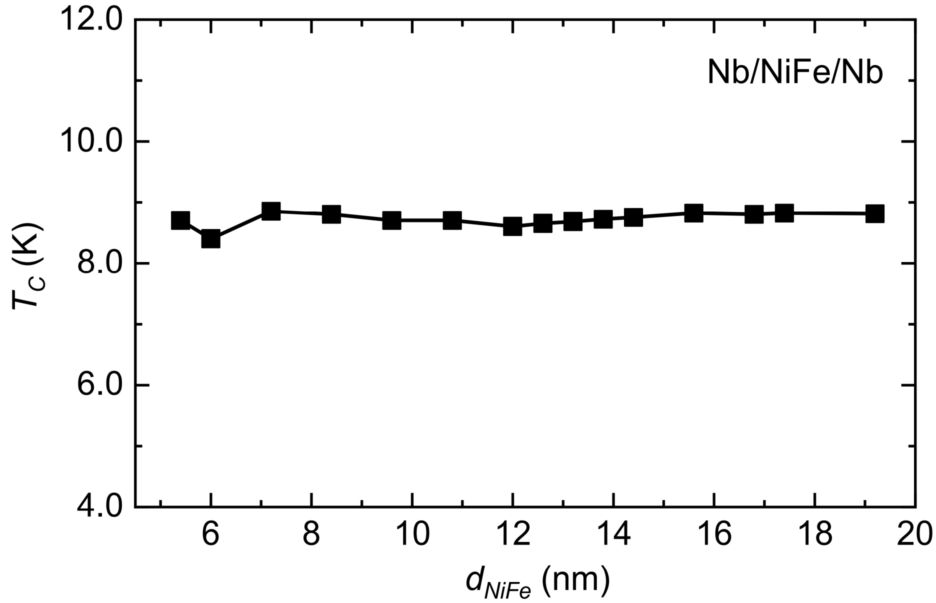

fig. S3. NiFe thickness dependence of T_C for the Nb/NiFe/Nb heterostructures. The T_C is determined from the zero-resistance temperature via four-probe resistance measurement.

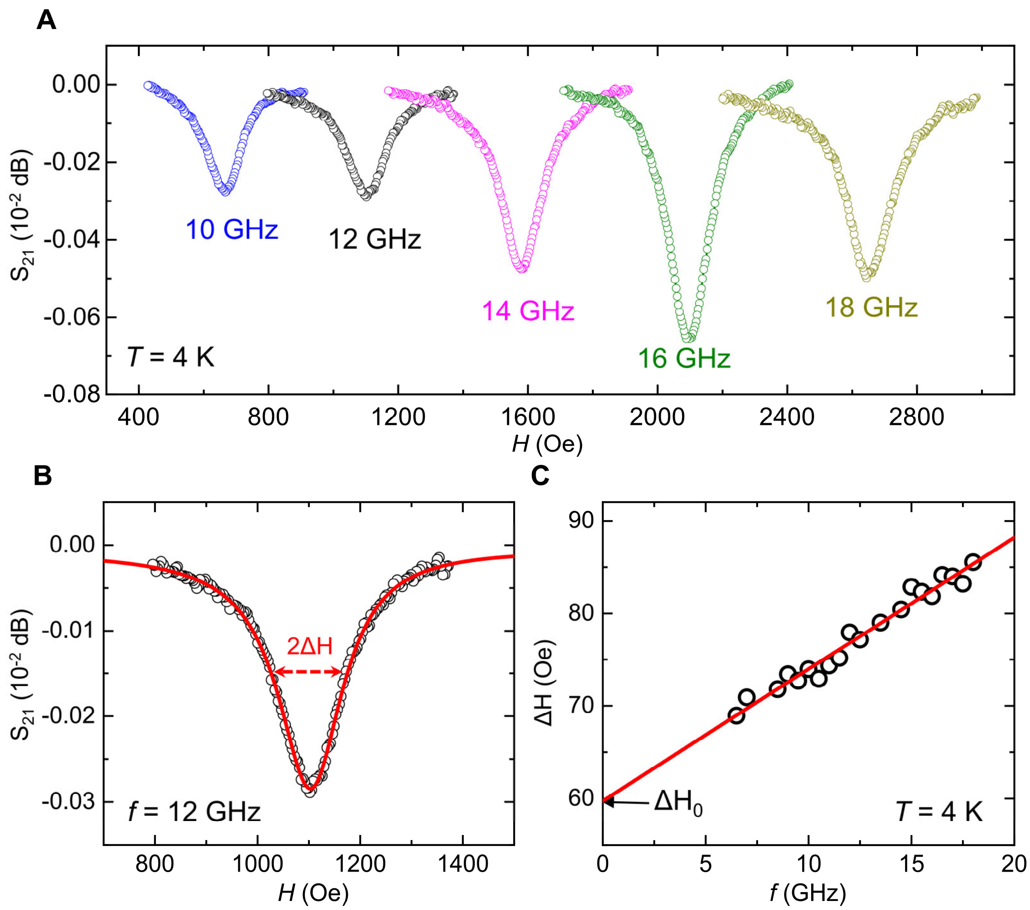

fig. S4. Measurement of the Gilbert damping of Nb/NiFe/Nb heterostructures at *T* = 4 K. (**A**) The typical FMR spectra as a function of magnetic field with microwave frequency (*f*) of 10, 12, 14, 16, and 18 GHz, respectively. (**B**) The typical FMR spectrum measured with *f* = 12 GHz (black circles) and the Lorentz fitting curve (red line). ΔH is the half linewidth of the FMR signal. (**C**) The determination of the Gilbert damping from ΔH vs. *f*. The red line indicates the best linear-fitting curve. These results are obtained on the typical Nb/Py (12 nm)/Nb sample.

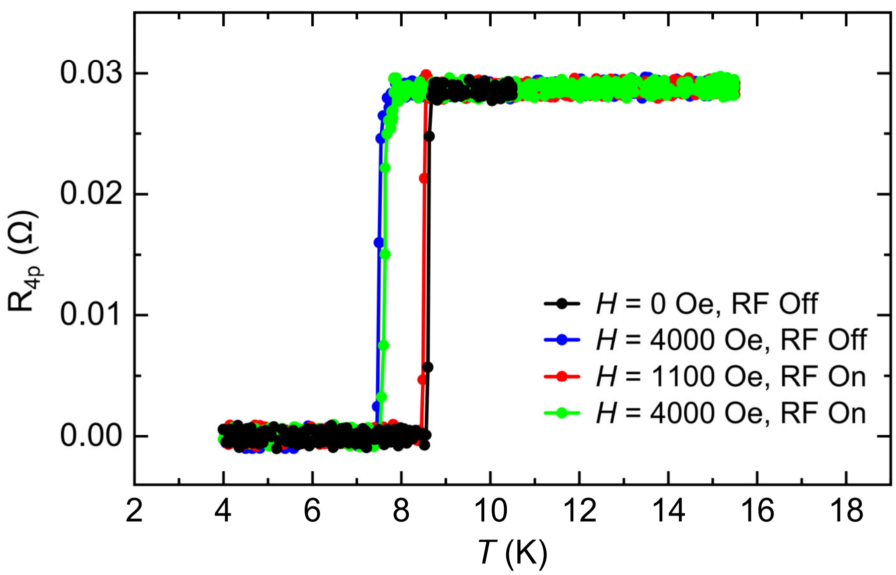

fig. S5. The effect of FMR measurement on the T_C of Nb/NiFe/Nb heterostructures. The four-probe resistances *vs.* temperature are probed from the typical Nb/NiFe (12 nm)/Nb sample with/without the presence of the in-plane magnetic field and microwave power.

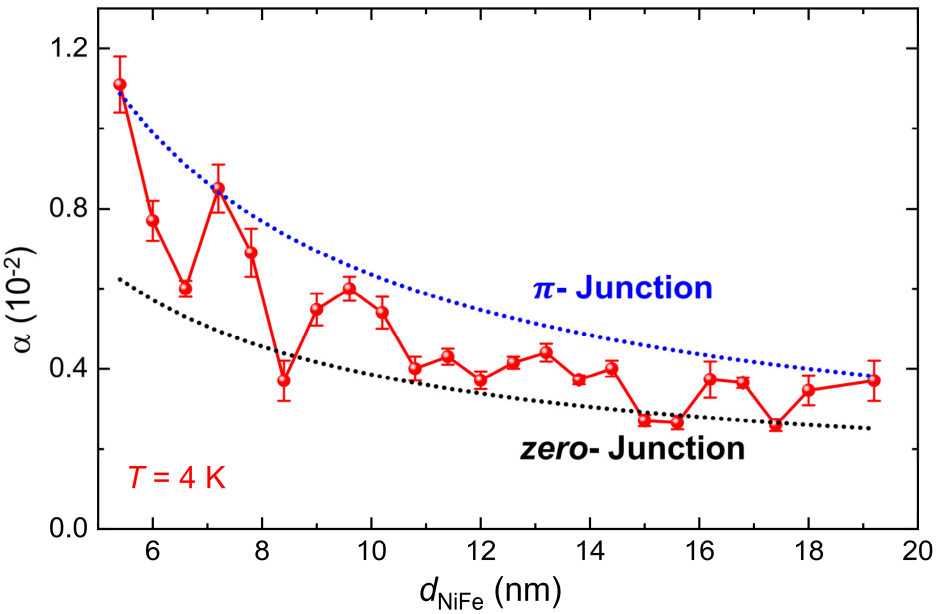

fig. S6. The Gilbert damping of *zero*- and π-junctions at $T = 4$ K. The solid balls represent the experimental data, the blue and black dash lines are the guide lines for π- and *zero*-junctions, respectively. For both guide lines, the damping is expected to behave as $\alpha \sim 1/d_{\mathrm{NiFe}}$. The Δα in main figure 4 represents Gilbert damping values of experimental data subtracted by those of the *zero*-junctions.

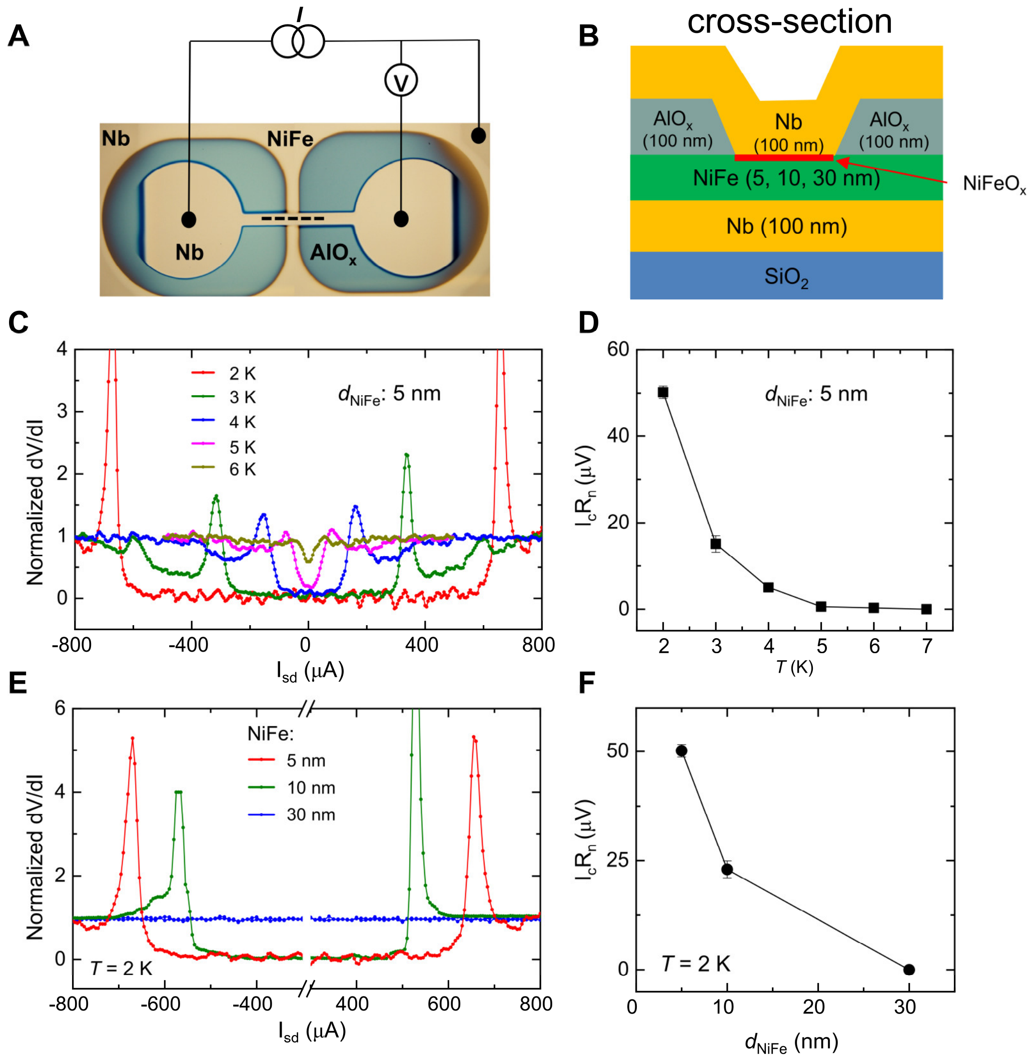

fig. S7. The measurement of Josephson coupling in Nb/NiFe/Nb junctions. (**A**) The optical image of a typical Nb/NiFe/Nb Josephson device and schematic of the electrical measurement geometry. (**B**) The cross-section of the Josephson devices with a junction area of ~ 80 μm × 80 μm. At the junction, a thin oxide layer of $NiFeO_x$ is mostly liked formed on the top surface of NiFe during the growth of AlO_x in the presence of oxygen. (**C**) The normalized differential resistance (dV/dI) as a function of the bias current measured on the Nb/NiFe (5 nm)/Nb junction from $T = 2$ to 6 K. (**D**) The temperature dependence of the characteristic voltage (I_cR_n) of the Nb/NiFe (5 nm)/Nb Josephson junction. (**E**) The normalized differential resistance as a function of the bias current of the Nb/NiFe/Nb junctions (d_{NiFe} = 5, 10 and 30 nm) at $T = 2$ K. (**F**) The NiFe thickness dependence of the characteristic voltages at $T = 2$ K.

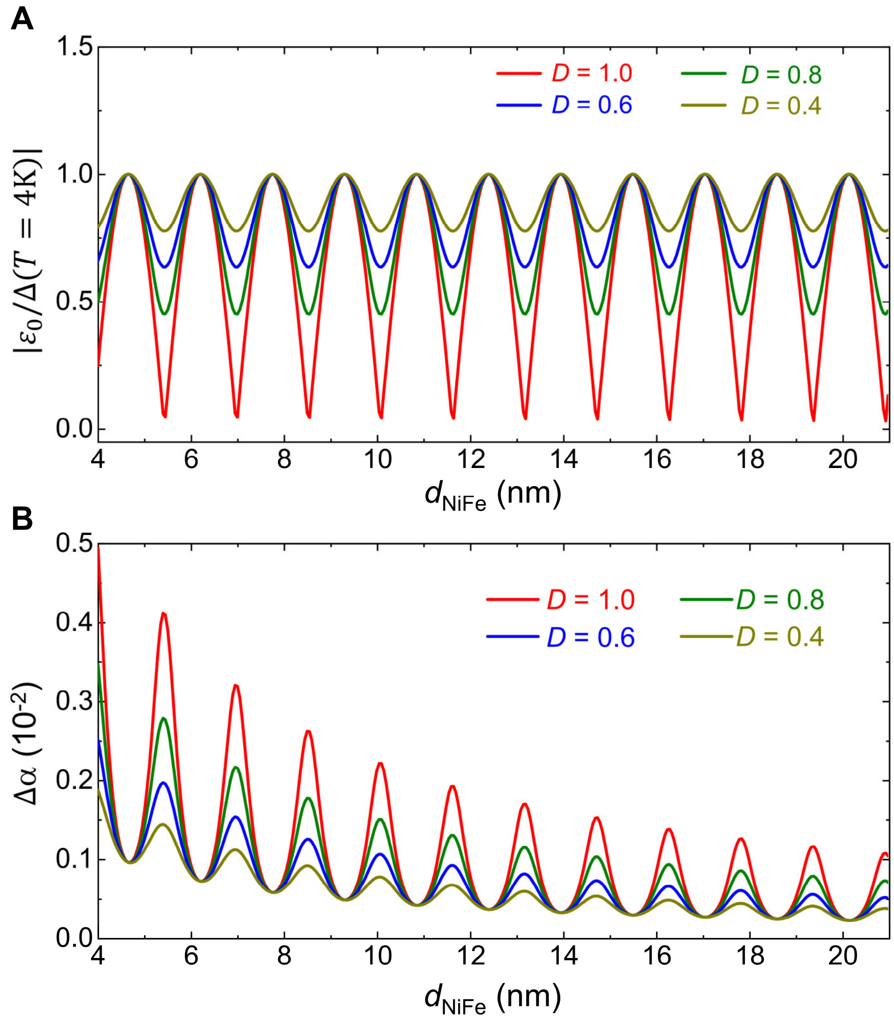

fig. S8. Calculation of the enhanced Gilbert damping due to spin pumping via the ABS at T = 4 K. (**A**) The normalized energy of ABS by the superconducting gap at T = 4 K as a function of d_{NiFe} with different transmission coefficients. (**B**) The enhanced Gilbert damping via ABS as a function of d_{NiFe} with different transmission coefficients. The red, green, blue, yellow, and orange solid lines represent the results with transmission coefficient D = 1.0, 0.8, 0.6, and 0.4, respectively.

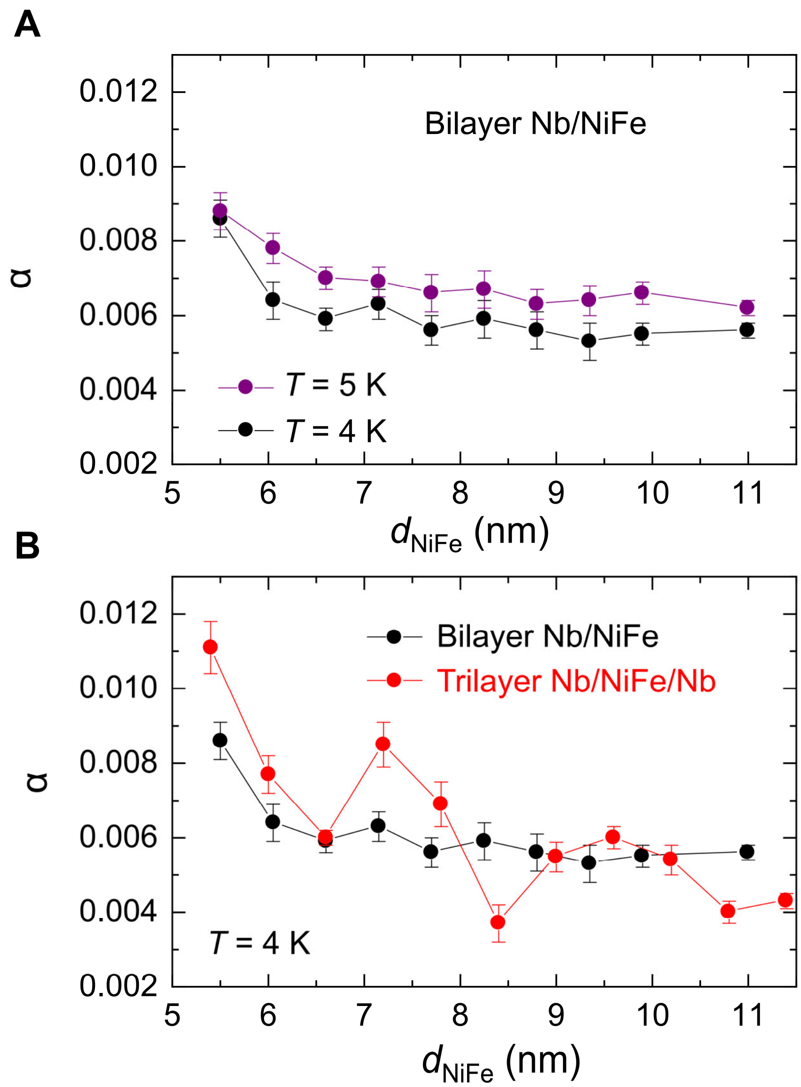

fig. S9. Gilbert damping of control sample of bilayer Nb/NiFe junctions. (A) Gilbert damping of bilayer Nb/NiFe junctions at $T = 4$ and 5 K. (**B)** Comparison of the Gilbert damping of bilayer Nb/NiFe and trilayer Nb/NiFe/Nb junctions at $T = 4$ K.